CAMBRIDGE
UNIVERSITY PRESS

Article

Composition and paragenesis of daqingshanite from the Kamthai carbothermalite, Rajasthan, India

Roger H. Mitchell 🔾

Department of Geology, Lakehead University, Thunder Bay, Ontario, Canada

Abstract

Daqingshanite in the Kamthai REE deposit (India) occurs as two paragenetic types: primary granular coarse grained crystals coexisting with primary carbocernaite, baryte and bastnäsite; and as aligned micro-ovoid globules within clasts of Sr-bearing calcite. Carbocernaite forming trellis-type lamellae in some of these calcite clasts do not represent exsolution and are considered as replacement textures as they formed subsequent to daqingshanite. The origins of the textural relations of the microglobules of daqingshanite to their host Sr-calcite cannot be unambiguously determined, although an exsolution origin is not considered feasible. The textures are similar to those of 'chalcopyrite disease' and as such could be interpreted as replacement features formed in a low temperature carbothermal environment which should facilitate replacement. Given that daqingshanite is an early crystallising phase it is also possible that cotectic crystallisation with Sr-calcite occurred, followed by subsolidus re-equilibration with recrystallisation along specific crystallographic planes in the calcite. The Kamthai REE deposit is best described as a low temperature carbothermalite microbreccia consisting of a wide variety of clasts resulting from the autobrecciation of rocks formed during, and after, the magmatic to carbothermal transition of an undetermined parental calcite carbonatite-forming magma. Many clasts have been replaced by late stage La-enriched carbothermal fluids mixed with exogenous water during the final low-temperature stage of evolution of the deposit.

Introduction

The mineral subsequently known as daqingshanite was described initially as unknown mineral UK44 from the Mont Saint-Hilaire intrusion in 1976 but could not be formally named due to the absence of a crystal structure determination. Eventually, this rare Sr–REE–P-bearing carbonate, was described and named from the Bayan Obo ore deposit by Yingchen *et al.* (1983). The mineral was further recognised in the Kamthai 'carbonatites' associated with the Sarnu-Dandhali alkaline complex, Rajasthan, India by Wall *et al.* (1993); an occurrence confirmed by R.H. Mitchell as noted in Bhushan and Kumar (2013) and Bhushan (2015). A further important discovery in the Nkombwa Hill carbonatite (Zambia), which eventually resulted in an accurate crystal structure determination, was reported by Appleton *et al.* (1992). Daqingshanite was found in the calcite-bearing groundmass of the Sover lamproite by Mitchell (1995) and recently the mineral has been recognised in the Kangankunde (Malawi) and Monteverde (Angola) fenites (Amores-Casals *et al.*, 2020, Dowman *et al.*, 2022) and the Sheep Creek REE deposit (Montana, USA) by Risedorf (2023).

The crystal structure of daqingshanite from Bayan Obo and Nkombwa Hill was determined by Ximen and Peng (1985) and Hughes and Yunxiang (1994), respectively. The high-precision crystal structure refinement of Hughes and Yunxiang (1994) established that the mineral was composed of alternating layers of Sr_3REE_1 and $(CO_3)_3(PO_4)_1$ resulting in a general formula which can be expressed as $A_3B_1C_1(CO_3)_3$ where: A = Sr, Ca, Ba, Na, K; B = La–Lu; and C = P, S.

The primary objective of this contribution is to provide new data on the composition and paragenesis of daqingshanite from Kamthai as this mineral has not been described, or discussed, in any of several recent publications (Patel *et al.*, 2023a, 2023b; Upadhyay *et al.*, 2021) concerned with the geology and mineralogy of this occurrence. It is not an objective of this work to provide a comprehensive petrogenetic model for the Kamthai REE occurrence and its relationships to the silicate rocks of the Sarnu-Dandhali complex, although some broad genetic relationships are considered on the basis of the evidence obtained in this study. Aspects of carbonatite nomenclature relevant to the Kamthai occurrence are described below.

Terminological note: carbothermalites

The carbonate rocks at Kamthai, following the initial descriptions by Bhushan and Kumar (2013), have been described in all subsequent publications (Patel *et al.*, 2023a, 2023b; Upadhyay *et al.*,

2021) as carbonatites (*sensu lato*). However, these rocks are actually better described as 'carbothermalites' following the criteria proposed by Mitchell (2005) and Mitchell and Gittins (2022), as they are composed of a complex assemblage of carbocernaite, bastnäsite, ancylite, baryte, strontian calcite and other minerals which are all formed at low temperatures from carbonate-dominated fluids subsequent to the magmatic to carbothermal transition of the parental magma (see below).

The use of the term carbothermal is preferred in this work, rather than carbonatite, as it describes a mineral assemblage dominated, with respect to the anions, by carbonates, fluorocarbonates, fluorides and sulfates rather than water-rich minerals. The term 'carbothermal solution' was used initially by Wall and Mariano (1996, p. 197) to refer to 'late carbonatites' enriched in rare earth elements (REE). Subsequently, Zaitsev *et al.* (1998, p. 248) recognised 'carbohydrothermal' fluids as forming the REE−Sr−Ba carbonate minerals in the Khibiny carbonatites. Wall and Zaitsev (2004, p. 347; their figure 10.1) presented a summary of compositional relations between common REE−Sr−Ba minerals, monazite and apatite in 'carbonatites' from which it is clear that occurrences dominated by REE-fluorocarbonates, carbocernaite, and burbankite represent assemblages formed from fluids with high carbonate/water ratios. Note that many investigations of REE−Sr−Ba mineralisation associated with alkaline rock complexes simply use the term 'hydrothermal' without consideration of the character of the mineral assemblages present. This approach can lead to assemblages dominated by water-poor REE−Sr−Ba carbonates being incorrectly termed 'hydrothermal' deposits. Consequently, Mitchell (2005) and Mitchell and Gittins (2022) recognised that there can be continuum between carbonate and water enriched residual magma/fluids, and that these can be described as carbothermal, carbohydrothermal, or hydrothermal depending on the carbonate/water ratios. In addition it is recognised that carbothermal fluids can evolve in some instances to *bona fide* hydrothermal fluids. Given that the principal REE−Sr−Ba mineral assemblage found at Kamthai is dominated by calcite, carbocernaite and daqingshanite, the term carbothermalite is used in this work to distinguish these rocks from earlier formed magmatic apatite calcite carbonatites (see the discussion section below).

Geological occurrence

The Kamthai Rare Earth Deposit (25°44'N, 71°52'E) is a member of the Tertiary Sarnu-Dandhali nepheline syenite–phonolite complex located in the Barmer District of Rajasthan. The geology of this complex is not well-known because of the extensive cover of the outcrops by the windblown sands of the Thar Desert. Aspects of the geology have been described by Bhushan (2015) and Bhushan and Kumar (2013) which indicate that, at the current level of exposure, the complex consists of a large body of nepheline syenite, small intrusions of ijolite breccia, scattered intrusions of the 'carbonatite complex', and numerous thin phonolite dykes. The latter cross-cut the carbonatite complex and an outcrop of ijolite but are older than the nepheline syenite. The 'carbonatite complex' consists of an initial irregular intrusion of calcite carbonatite and numerous thin younger Ba−Sr−REE enriched carbonate dyke-like intrusions. The latter also occur as isolated irregular dykes which cross-cut an ijolite intrusion.

Although the Kamthai REE-vein deposits are associated geographically with alkaline silicate rocks, interpretation of their relationships and genesis is hindered by the very poor exposure and paucity of petrological investigations. Clearly, the Sarnu-Dandhali alkaline complex has similarities with other alkaline rock carbonatite complexes in that they contain ijolites, nephelinites and phonolites, but documentation of the exact relationships with potential carbonatite-forming magmas such as nephelinite are not available. Recently, Mahala and Ray (2022) have determined that the Sr and Nd isotopic compositions and ages of the alkaline rocks and carbothermalites are similar and concluded that they are probably genetically related. However, Mahala and Ray (2022) did not provide any genetic model apart from some generalisations considering all the rocks to be related by either fractional crystallisation or liquid immiscibility.

The Kamthai REE deposit is notable for the presence of abundant carbocernaite, britholite, Sr-baryte, strontianite and rare earth element carbonates enriched in La: i.e. bastnäsite-(La) and ancylite-(La). The presence of daqingshanite at Kamthai was recognised initially by Wall *et al.* (1993), who illustrated small (c. 10×50 μm) anhedral crystals associated with later-forming carbocernaite. Daqingshanite-bearing rocks which have not been subjected to extensive secondary carbohydrothermal alteration in terms of their modal mineralogy are best termed baryte bastnäsite carbocernaite carbothermalites (see below). Note that Patel *et al.* (2023b) provided a paragenetic sequence for the carbothermalites which inexplicably does not include daqingshanite.

Standard optical and back-scattered electron (BSE) petrographic observations (this work; Bhushan, 2015; Patel *et al.*, 2023a, 2023b) show clearly that the Kamthai REE carbothermal vein deposit, referred to as a 'late carbonatite' by Wall and Mariano (1996), as a whole does not exhibit the typical textures or mineralogy of primary magmatic carbonatites as defined by Mitchell and Gittins (2022). However, such carbonatites form the irregular earlier calcite carbonatite plug and occur as clasts within the REE-enriched carbothermal deposit. The latter is here considered as a carbothermal microbreccia consisting of veins and clasts with a wide range of textural and mineralogical characteristics.

The Kamthai carbothermalites (*sensu lato*) are fine grained microbreccias which exhibit extra-ordinarily complex dissolution, re-precipitation and secondary replacement textures. Data given by Patel *et al.* (2023a) show that Kamthai calcite exhibits a very wide range of textural and compositional types that actually cannot always be placed objectively in any simple paragenetic sequence, although they suggest that there is a broad division between 'magmatic' and 'hydrothermal' assemblages. These have been described by Patel *et al.* (2023a, 2023b) and Upadhyay *et al.* (2021), who claim that diverse 'primary' and 'secondary mineral assemblages' can be recognised. Primary assemblages are considered by Patel *et al.* (2023b) to include Sr-bearing calcite (3–12 wt.% SrO) termed 'magmatic calcite' although this interpretation appears to include magmatic and carbothermal calcite compositions, and is based upon the incorrect assumption that all primary calcite must be Sr rich. However, given that most of the calcite in the carbothermalite breccias do not have the allotriomorphic granular textures or compositional features of the low Sr contents of *bona fide* magmatic calcite these are best described as carbothermal calcite. Note that some of the carbothermal calcite investigated in this work would be considered as 'magmatic' by Patel *et al.* (2023a, 2023b).

Analytical methods

Polished thin sections of nine grab samples of carbothermal microbreccia provided by Ramgad Minerals were examined by

back-scattered electron petrography as standard optical petrographic methods are not suitable for these fine grained texturally-complex materials. Compositions of the phases present were determined by quantitative energy-dispersive X-ray spectrometry using a Hitachi FE-SU70 scanning electron microscope (SEM) equipped with an Oxford Instruments X-MAX 80mm^2 Si-drift detector and the *AZtec* software package. The electron accelerating voltage was 20 kV and the beam current 300 pA. Standards used were: wollastonite (Si,Ca); corundum (Al); jadeite (Na,Al); BaF$_2$ (Ba, F); Mn-hortonolite (Mg, Fe, Si, Mn); synthetic rare element phosphates (La, Ce, Pr, Nd, Sm, P); SrTiO$_3$ (Sr, Ti); ThNb$_4$O$_{12}$ (Th, Nb); and ilmenite (Ti, Fe). The rastered beam (15×15 μm) and low beam currents (300 pA) employed for quantitative X-ray energy-dispersive spectrometric (EDS) analysis permitted accurate and reproducible analysis of small crystals in a variety of hosts without excitation of the latter. Note that the brightness and contrast settings of BSE detectors are critical in distinguishing daqingshanite from associated carbocernaite and britholite.

It is important to note that analysis of alkali-REE-carbonates requires that a low beam current coupled with rastering of the analytical site must be employed if alkali loss is to be avoided. Supplementary Fig. 1 demonstrates that spot analyses of carbocernaite for a live time of 60 s (30% dead time) with a 300 pA beam current, results in significant beam damage whereas rastering causes no obvious damage during the same irradiation time. Several spot analyses resulted on average in a 61% decrease in the Na content of the carbocernaite whereas there was no change in the Na content for a 15 × 15 μm area with rastered analysis. Similar effects were observed for the analysis of ancylite. It is well-known that analysis of carbocernaite by electron microprobe analyses methods requires electron beam defocussing to ~10 μm to avoid Na loss with beam currents of 20 nA (Chakhmouradian *et al.*, 2017). From these observations and the above it is apparent that the compositions of carbocernaite given by Patel *et al.* (2023a) using a 50 nA beam current, even with defocussing (1–15 μm), reflect significant alkali loss resulting in significant *A*-site cation deficiencies. Hence, Na$_2$O contents reported by Patel *et al.* (2023a) range from 0.1–2.8 wt.%; i.e. considerably less than typical carbocernaite compositions which vary from 2.5–5.4 wt.% Na$_2$O, with the majority in the range of 3–5 wt.% (Wall *et al.*, 1993; Zaitsev *et al.*, 1998; Chakhmouradian *et al.*, 2017; Sitinikova *et al.*, 2021).

Daqingshanite paragenesis and composition

Daqingshanite in some of the Kamthai carbothermalites, which have not been subjected to extensive later carbohydrothermal alteration, occurs in two textural-paragenetic types: (1) anhedral coarse grained primary crystals associated with britholite, carbocernaite and baryte; (2) very small ovoid-to-round microcrystalline inclusions in Sr-rich calcite clasts, which in some instances, are characterised by trellis-textured lamellae of carbocernaite occupying the rhombohedral cleavage planes of the calcite.

Paragenetic type 1 paragenesis

The typical paragenesis of daqingshanite which occurs as abundant anhedral-to-rounded crystals surrounded by large interlocking anhedral crystals of carbocernaite, commonly with associated contemporaneous baryte and bastnäsite (see below) is illustrated in Fig. 1. The daqingshanite contains rounded inclusions of
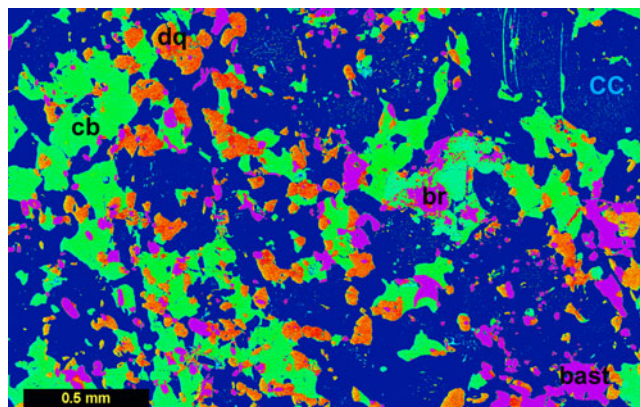

Figure 1. Paragenetic relationships between britholite (br), daqingshanite (dq) and carbocernaite (cb). False colour BSE image emphasising the sequence of crystallisation of these three minerals. All are set in a colour-undifferentiated matrix of diverse calcite (cc).

britholite and rarer monazite-(La). Clusters of anhedral large daqingshanite crystals of variable composition which have crystallised prior to carbocernaite are illustrated in Fig. 2. The late-forming matrix is strontian calcite of diverse composition (8–12 wt.% SrO). Britholite is present as earlier-formed rounded inclusions in daqingshanite. Figure 3 shows daqingshanite which has apparently crystallised in association with ancylite together with oscillatory zoned Ca–Fe–Mn carbonate (14–29 wt.% FeO; 19–31 wt.% MnO; 9–13 wt.% CaO). Daqingshanite also occurs as anhedral single crystals within the strontian calcite matrix. These are interpreted to represent material derived by the disaggregation of previously formed aggregates of daqingshanite crystals.

Paragenetic type 1 composition

Typically, Kamthai daqingshanite is enriched in the light rare earth elements (REE) although these are not dominant over Sr. No data are available for the heavy REE or other trace elements. Hughes and Yunxiang (1994) consider that there is little or no
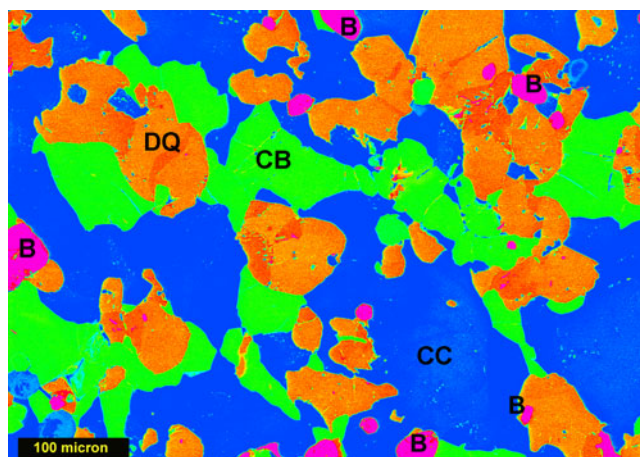

Figure 2. False colour BSE image of anhedral, resorbed and compositionally zoned coarse grained daqingshanite (DQ) overgrown by carbocernaite (CB) of uniform composition set in a colour-undifferentiated matrix of diverse calcite (CC).
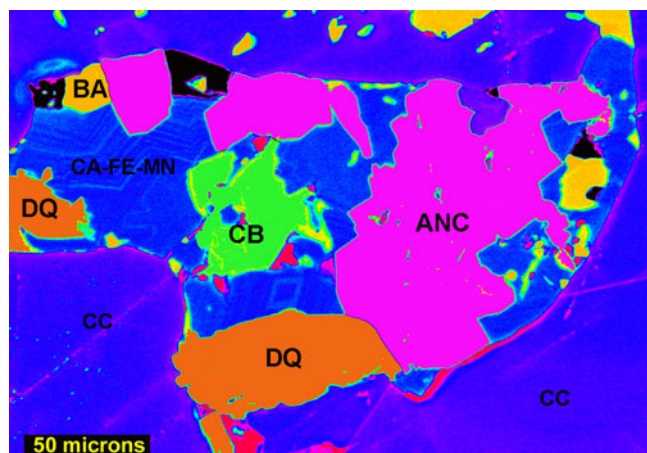
Figure 3. False colour BSE image of a clast showing the paragenetic relationships between early-formed daqingshanite (DQ) and carbocernaite (CB) set in a matrix of ancylite (ANC), baryte (BAR) and Ca–Fe–Mn carbonates of diverse composition. The clast is set in matrix of Sr-poor calcite (CC).

Figure 4. False colour BSE image illustrating the compositional zoning in primary granular daqingshanite.

substitution of hydroxyl ions or fluorine in the structure. Supplementary Fig. 2 illustrates the composition of Kamthai daqingshanite as determined by energy-dispersive X-ray spectrometry which shows clearly the presence of Na, K and S and the absence of Cl. Although a small peak attributable to $FK\alpha$ is also present this cannot be resolved using SEM-EDS to give a satisfactory analytical accuracy or precision due to significant overlaps with low energy REE and oxygen peaks. It is estimated, using 120 s counting time, that F is present near the limits of detection at contents of 0.3–0.4 wt.%. These amounts are insignificant with respect to the structural formulae of daqingshanite calculated on the basis of three carbonate groups.
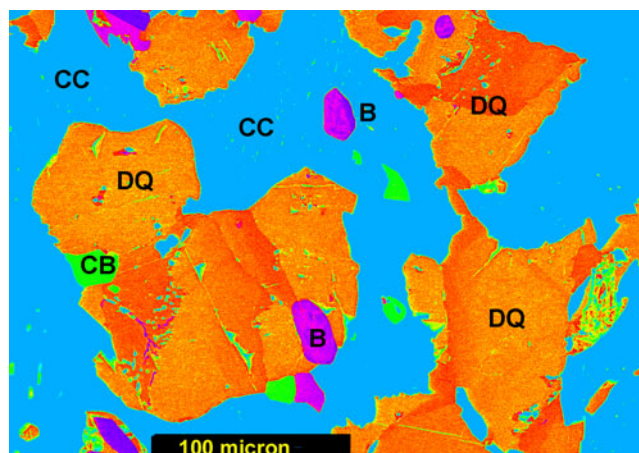
The composition of Kamthai daqingshanite was established initially by Wall *et al.* (1993) who noted the significant differences to the type locality material from Bayan Obo which is significantly enriched in Ba (Table 1; comp. 9), has lower REE contents and that S is present (Table 1; comp. 8). Although Appleton *et al.* (1992) did not determine the S content of Nkombwa daqingshanite, their data (Table 1; comp.8) included F (0.29 wt.%) and Cl (0.10 wt.%).

Examples of the compositional zoning of Kamthai daqingshanite as illustrated by back-scattered electron (BSE) imagery are shown in Fig. 4. Simple core-to-rim variation is not evident in the majority of the crystals although instances of internal compositional gradients are evident. These, and the well-defined compositional boundaries, within other parts of the crystal are attributed

Table 1. Representative compositions of daqingshanite.

Wt.%	1	2	3	4	5	6	7	8	9
Na_2O	0.36	0.40	0.48	0.26	bld	bld	bld	bld	0.13
K_2O	0.49	0.46	0.50	0.34	0.34	0.19	bld	bld	bld
CaO	9.15	9.24	9.00	8.42	6.33	5.85	7.75	6.94	6.17
SrO	26.71	27.60	29.16	32.08	33.27	35.23	33.41	41.82	26.10
BaO	1.79	2.10	2.05	1.99	1.83	1.91	3.17	4.57	15.98
La_2O_3	11.57	13.60	12.22	10.54	11.75	11.25	10.97	10.22	7.88
Ce_2O_3	12.32	12.41	13.03	12.84	12.70	12.11	10.91	12.24	10.60
Pr_2O_3	0.79	0.90	0.99	1.02	0.98	0.71	bld	0.83	0.68
Nd_2O_3	1.53	1.44	1.75	1.92	1.51	1.79	1.53	1.71	1.59
P_2O_5	8.11	8.26	8.14	9.05	9.88	9.55	8.82	10.50	11.73
SO_3	0.89	0.99	0.71	0.55	0.14	0.11	0.42	nd	nd
Total	74.11	77.40	78.63	79.01	78.73	78.70	76.78	82.82	80.86
Structural formulae calculated on the basis of 5 cations in apfu									
Na	0.079	0.085	0.101	0.054	-	-	-	-	0.028
K	0.035	0.082	0.034	0.023	0.024	0.013	-	-	-
Ca	1.107	1.086	1.042	0.963	0.748	0.693	0.917	0.112	0.772
Sr	1.748	1.756	1.826	1.986	2.127	2.259	2.139	2.689	1.652
Ba	0.079	0.090	0.087	0.083	0.079	0.083	0.137	0.198	0.684
A-site	*3.048*	*3.050*	*3.090*	*3.109*	*2.977*	*3.048*	*3.193*	*2.988*	*3.086*
La	0.498	0.510	0.487	0.415	0.478	0.459	0.447	0.418	0.317
Ce	0.509	0.499	0.515	0.502	0.513	0.490	0.441	0.497	0.424
Pr	0.032	0.036	0.039	0.040	0.039	0.029	-	0.034	0.027
Nd	0.062	0.056	0.068	0.073	0.059	0.071	0.060	0.068	0.062
B-site	*1.102*	*1.101*	*1.109*	*1.030*	*1.089*	*1.048*	*0.948*	*1.106*	*0.830*
P	0.775	0.767	0.744	0.818	0.922	0.894	0.824	0.986	1.084
S	0.075	0.082	0.058	0.044	0.012	0.009	0.035	-	-
C-site	*0.850*	*0.849*	*0.802*	*0.862*	*0.934*	*0.903*	*0.859*	*0.986*	*1.084*

bdl – below detection limit; nd – not detected

to sector zoning. Representative compositions of the zones are given in Table 1. Those with high BSE contrast (dark orange in Figs 2 and 4) are enriched in Sr and P relative to other regions of the crystals with low BSE contrast and are depleted in Ba, Na, K and S, although none of the compositions are as enriched in Sr or Ba as the Nkombwa and Bayan Obo material (Table 1). Primary daqingshanite from the Sheep Creek carbothermalite (Risedorf, 2023) is relatively Ba-rich (4.5–7.1 BaO wt.%) but Sr and REE-poor (in wt.%: 26–28 SrO; 9.9–13.5 La$_2$O$_3$; 11.8–13.59 Ce$_2$O$_3$) compared to Kamthai daqingshanite. Daqingshanite from Nkombwa and Sover are Sr-rich, whereas that from Bayan Obo is relatively Ba-rich. From Fig. 5 it is evident that daqingshanite can exhibit significant compositional variation especially with respect to Ca, Sr and Ba contents, and it is suggested that both the Ba and Ca end-member compositions might exist in Nature or can be synthesised.

Paragenetic type 2

Paragenetic type 2 occurs as very small (typically <10 μm) discrete ovoid globules set in Sr-rich calcite (in wt.%: 10–12 SrO; 2–3 MnO; 0.4–0.5 BaO; ~0.5 MgO) matrices. Two textural varieties are present. In both of these, the daqingshanite globules have a subparallel well-defined orientation that does not follow any obvious crystallographic planes (see below).

In one textural variety (Fig. 6a,b), other minerals are rare-to-absent, although single anhedral crystals of carbocernaite, Cr-rich strontianite, daqingshanite, britholite and Al–Mn-bearing magnetite, lacking any preferred orientation relative to the globules can be found (Fig. 6c). BSE petrography demonstrates that these daqingshanite–strontian calcite assemblages represent single clasts set in a Sr-rich calcite matrix that lacks globular daqingshanite (Fig. 6a). This cementing calcite is poorer in SrO (7–10 wt.%) and MgO (<0.3 wt.%) than that of the clasts.

Another type of clast characterised by daqingshanite globules is illustrated in Fig. 7. These are characterised by a network of thin carbocernaite lamellae. In some clasts these lamellae form a trellis-like intergrowth of two sets of parallel lamellae which apparently follow the rhombohedral cleavage of the Sr-calcite host (Fig. 7a). It is to be noted particularly that the orientation
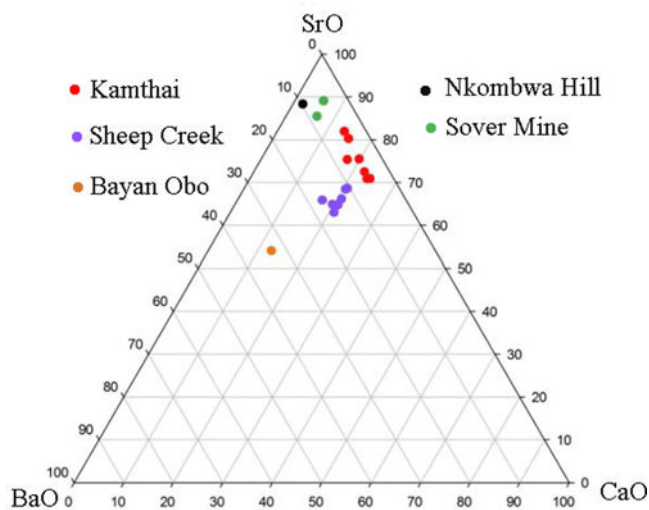

Figure 5. Compositions of daqingshanite expressed in the ternary system CaO–SrO–BaO. Data from: this work; Yingchen *et al.* (1983); Wall, *et al.* (1993); Appleton *et al.* (1992); Mitchell (1995); and Risedorf (2023).
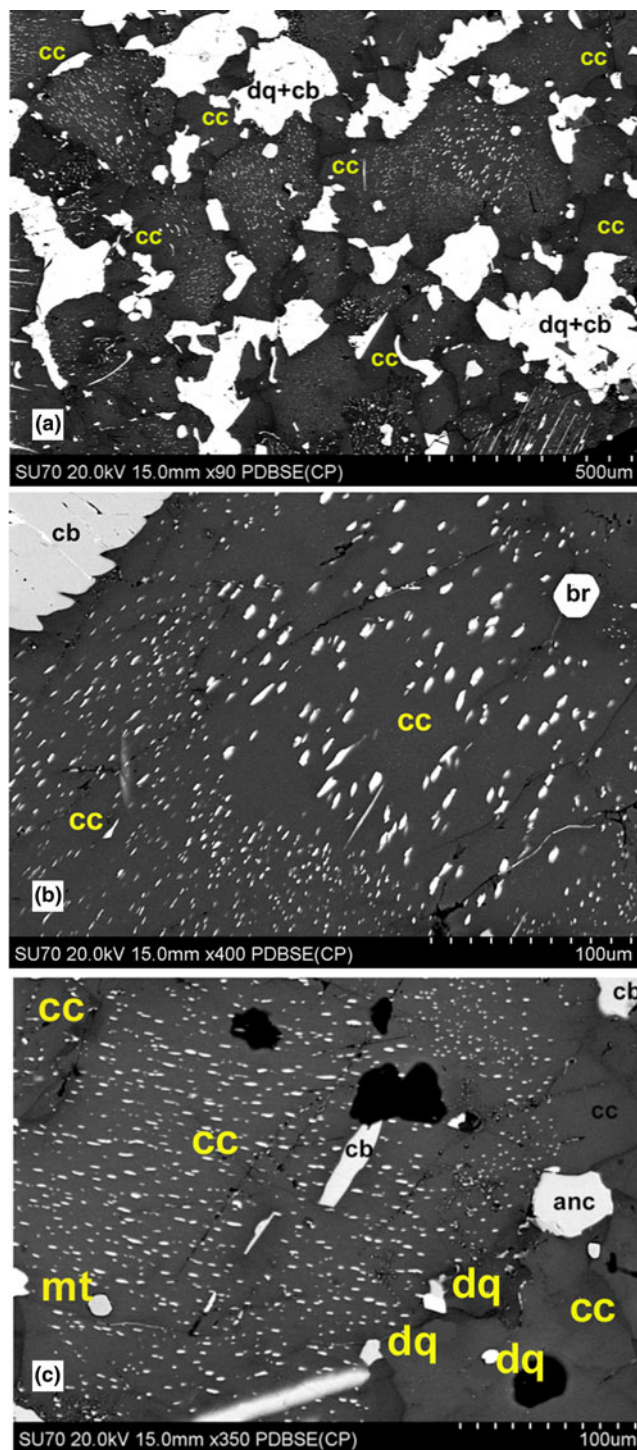

Figure 6. BSE images of: (a) Microbreccia with clasts of type 2 daqingshanite plus carbocernaite (dq+cb), and clasts of type 2 micro-globular daqingshanite set in a Sr-calcite matrix. All clasts are cemented in a matrix of Sr-calcite; (b) Composite clast of micro-globular type 2 daqingshanite (white) set in Sr-calcite (cc) with isolated antecryst of resorbed britholite (br); (c) Clast of micro-globular daqingshanite (white) set in Sr-calcite containing antecrystal carbocernaite (cb). The clast is set in a cement of Sr-calcite which contains resorbed antecrysts of granular type 1 daqingshanite (dq) and ancylite (anc).

of the carbocernaite lamellae is not the same as that of the daqingshanite globules, and that carbocernaite lamellae cross-cut these globules (Fig. 7b). In other clasts, depending upon their
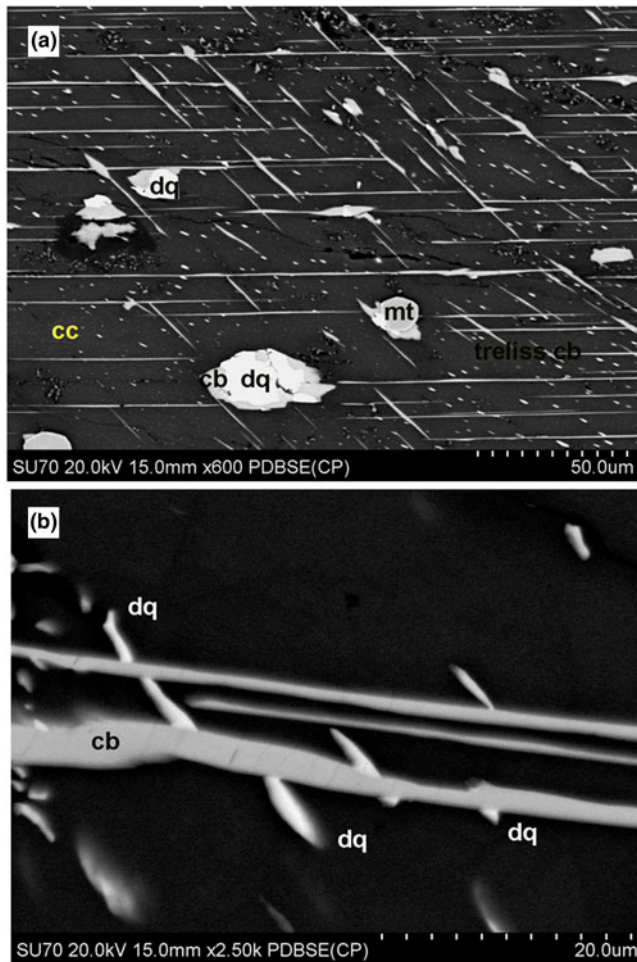
Figure 7. BSE images of: (a) lamellae carbocernaite and micro-globular type 2 daqingshanite set in Sr-calcite matrix with resorbed antecrysts of type 1 daqingshanite (dq), carbocernaite (cb) and magnetite (mt). Note that the orientation of the daqingshanite ovoids is not the same as that of the carbocernaite lamellae: (b) Illustration of carbocernaite lamella cross-cutting micro-ovoids of type 2 daqingshanite. Dark matrix is Sr-calcite.

Figure 8. False colour BSE images of: (a) Replacement carbocernaite lamellae (cb) with antecrystal britholite (br), pyrite (py) and baryte (ba) set in a Sr-calcite matrix showing secondary replacement textures (a). (b) Detail of the secondary replacements showing that they are composed of a intimate intergrowth of calcian strontianite (green) and strontian calcite (dark blue). Also present are carbocernaite lamella (cb) showing replacement textures with matrix calcite (cc) and antecrysts of britholite which have been transported with carbocernaite during the emplacement of the lamellae.

orientation, only one set of lamellae is evident, in others flame-like structures emanate from the lamellae (Fig. 8a). In some examples lamellae are curved and/or form symplectite-like intergrowths. The carbocernaite lamellae in some instances contain single crystals of daqingshanite, Al–Mn magnetite, baryte and britholite (Fig. 8a). The Sr-calcite (11–12 wt.% SrO) host to all varieties is similar to that of clasts lacking carbocernaite lamellae.

The strontian calcite matrices of both types of clasts also commonly exhibit replacement by many small (< 30 μm) of amoeboid-like fine grained intergrowths (Fig. 8a,b). Although these are too small for accurate analysis it is apparent that they consist of Ba–Mn-bearing Sr-calcite (in wt.%: c. 28.5 SrO; c. 1.0 BaO; 1 MnO) intergrown with relatively Sr-poor calcite (c. 12 wt.% SrO) enriched in MgO (0.4 wt.%), MnO (c. 2 wt.% and REE (0.9 La_2O_3 wt.%; 1.7 wt.% Ce_2O_3). Patel *et al* (2023a) describe these as secondary carbocernaite although the crystals in the intergrowths are actually too small for accurate EMPA.

Globule daqingshanite composition

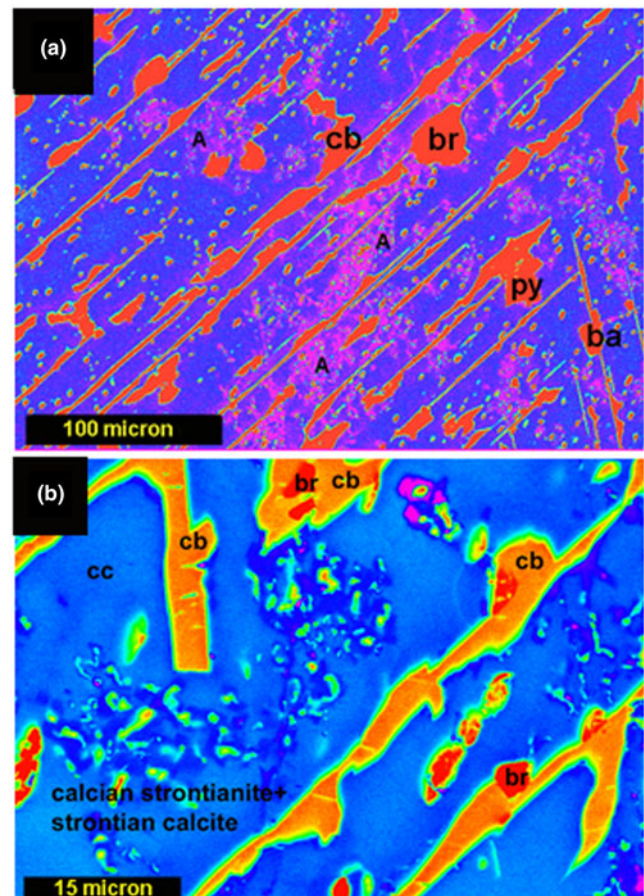Because of their small size, determination of the composition of the globules is very difficult due to excitation of the host Sr-calcite. Rare examples with larger size (c. 15–20 μm) can be found which give reasonable rastered analytical totals and P, REE and Sr contents (Table 2). These data indicate that the globules have compositions which are very similar to the granular type 1 daqingshanite. However, even for these crystals, matrix excitation of Ca cannot be ruled out.

Table 2. Composition of globular daqingshanite.

Wt.%	1	2	3	4
Na_2O	0.41	0.59	0.35	bld
K_2O	0.62	0.97	0.72	0.22
CaO	8.49	7.83	11.01	11.22
SrO	27.92	30.03	30.19	32.92
BaO	2.34	3.03	2.35	1.94
La_2O_3	12.19	12.48	12.10	8.74
Ce_2O_3	11.64	12.83	11.97	11.58
Pr_2O_3	1.05	0.70	0.99	0.83
Nd_2O_3	1.36	1.35	1.36	1.96
P_2O_5	7.48	6.32	7.02	8.53
SO_3	0.93	1.05	0.95	1.78
Total	74.43	77.18	79.01	79.72

bdl – below detection limit

Carbocernaite

Paragenesis

Carbocernaite, is a major component of the material investigated, and occurs intergrown with daqingshanite as anhedral granular crystals set in a Sr-calcite matrix (Figs 1–3), large anhedral granular clusters in clasts, and as diverse lamellae in daqingshanite–Sr-rich calcite clasts (Figs 7, 8). BSE petrography shows that in all cases carbocernaite has crystallised subsequent to daqingshanite but has not pseudomorphed this mineral. Pseudomorphs after burbankite are not present. Isolated anhedral crystals of carbocernaite in diverse matrices represent disaggregated granular aggregates of the type shown in Fig. 2. During the formation of lamellae some carbocernaite appears to have transported other minerals (daqingshanite, magnetite, britholite and pyrochlore) along the lamellae. A common assemblage found in the material investigated consists of apparently contemporaneously crystallising carbocernaite, Sr-baryte and bastnäsite-(La). All carbocernaite types appear to have formed prior to the Sr-rich calcite matrices.

Carbocernaite is known to occur in carbonatites and/or carbothermalites in a wide variety of textural types: discrete crystals and clusters; supposed exsolution lamellae in calcite; pseudomorphs after burbankite, calcite or ferroan dolomite; and overgrowths on cordylite (Chakhmouradian *et al.*, 2017). The bulk of the Kamthai carbocernaite occurs as discrete crystals and overgrowths on daqingshanite and its formation during the early stages of crystallisation is unquestionable. The origins of the trellis lamellae carbocernaite are less easily determined and although these have the appearance of trellis exsolution they exhibit features at variance with this process which are discussed below.

Composition

The structure of carbocernaite has been determined by Shi *et al* (1982) and Chakhmouradian *et al.* (2017) and the ideal composition is $(Ca,Na)(Sr,Ce,Ba)(CO_3)_2$. Representative compositions and structural formulae of Kamthai carbocernaite are given in Table 3 which demonstrates, in accord with BSE imagery

(Figs 2–5), that there is very little compositional variation in the material investigated. In contrast to Wall *et al.* (1993), who report Na-poor lamellae in calcite, there are no significant compositional differences between granular and lamellae carbocernaite. These compositions are very similar to carbocernaite from Khibina, Russia (Zaitsev *et al.*, 1998) and Bear Lodge, Wyoming, USA (Chakhmouradian *et al.*, 2017), all of which have La/Ce < 1 in contrast to the data of Wall *et al.* (1993) which have La/Ce >1 (Table 3 comp. 11) or Patel *et al.* (2023a) for which there are La/Ce ratios varying from less than, to greater than, unity. As noted above, all data given by Patel *et al.* (2023a) are deficient in Na, ranging from 0.4–2.8 wt.% Na_2O (Table 3; comps. 9 and 10), and are considered to be inaccurate due to extensive Na loss under the extremely high electron beam currents employed for analysis (see methodology above) and are not discussed further.

Britholite

Britholite $(REE,Ca,Sr)_5(SiO_4,PO_4)_3(OH,F)$ is commonly found as ovoid inclusions in daqingshanite (Fig. 2) and carbocernaite, as aggregates of anhedral crystals in bastnäsite-(La) (Fig. 9) and as single anhedral crystals in Sr-calcite which are undoubtedly derived by disaggregation of such aggregates. All britholite is altered and characterised by irregular and heterogeneous regions of different BSE contrast (Fig. 9). Euhedral crystals of britholite are not found and it is evident from the texture that britholite, and monazite, have been resorbed prior to incorporation into all other minerals present in the Kamthai carbothermalites.

Representative compositions of britholite are presented in Table 4. Regions of high BSE contrast (darker orange in Fig. 9) are enriched in Si and REE relative to regions of low BSE contrast which are relatively enriched in P and Ca. These compositional variations reflect substitutions in the well-known britholite–apatite solid-solution series. Although all britholite analysed contains F (0.4–1.0 wt.%), analytical totals are low reflecting the presence of significant amounts of OH (Table 4). Thus, the mineral here is best referred to as 'hydroxylbritholite'. Previous

Table 3. Representative compositions of carbocernaite.*

wt.%	1	2	3	4	5	6	7	8	9	10	11
Na_2O	3.25	3.43	3.54	3.80	3.97	3.40	3.50	3.77	0.44	2.84	4.11
CaO	16.53	16.88	16.48	16.44	15.75	16.43	16.96	16.39	15.59	14.89	16.95
SrO	23.90	22.66	24.23	21.59	20.89	21.72	22.67	21.88	24.45	19.95	21.36
BaO	1.13	1.09	1.18	0.98	0.82	1.34	1.71	1.45	0.98	0.20	1.44
La_2O_3	8.05	8.01	8.99	9.35	10.16	7.98	8.35	9.01	10.36	11.42	11.77
Ce_2O_3	8.40	8.91	9.82	9.67	10.18	9.23	9.02	9.86	11.39	14.20	9.72
Pr_2O_3	0.84	0.84	0.83	0.63	0.79	0.75	0.57	0.71	1.09	1.28	0.75
Nd_2O_3	1.33	0.95	0.88	0.92	0.80	1.07	0.72	0.91	1.97	2.46	1.98
Total	63.67	64.21	65.95	63.55	63.59	63.51	63.72	64.23	66.27	67.24	68.36
Structural formulae in apfu calculated on the basis of 2 $(CO_3)^{2-}$ groups											
Na	0.278	0.294	0.293	0.324	0.340	0.296	0.297	0.320	0.037	0.237	0.329
Ca	0.780	0.799	0.753	0.774	0.746	0.791	0.796	0.768	0.733	0.686	0.750
A site	1.058	1.093	1.046	1.098	1.086	1.087	1.093	1.088	0.770	0.923	1.079
Sr	0.610	0.580	0.599	0.550	0.536	0.566	0.576	0.555	0.692	0.498	0.512
Ba	0.020	0.019	0.020	0.017	0.014	0.024	0.029	0.025	0.017	0.003	0.023
La	0.131	0.131	0.141	0.152	0.166	0.132	0.135	0.145	0.168	0.181	0.179
Ce	0.135	0.144	0.153	0.156	0.165	0.152	0.145	0.158	0.190	0.224	0.147
Pr	0.013	0.014	0.013	0.010	0.013	0.012	0.009	0.011	0.017	0.020	0.011
Nd	0.021	0.015	0.013	0.014	0.013	0.017	0.011	0.014	0.031	0.038	0.029
B site	0.930	0.903	0.939	0.899	0.907	0.903	0.905	0.908	1.115	0.964	0.901

*Compositions: 1–5 granular carbocernaite with daqingshanite; 6–8 lamella carbocernaite in calcite (this work); 9–10 from Patel *et al.* (2023a); 11 granular carbocernaite with britholite (Wall *et al.*, 1993).
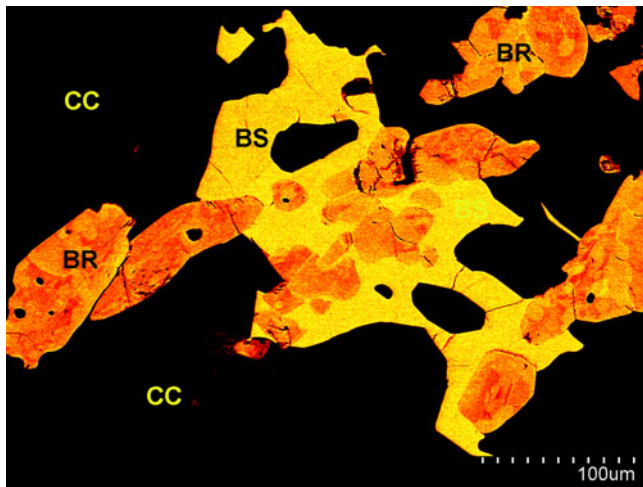
Figure 9. False colour BSE image of resorbed and compositionally zoned britholite set in a matrix of bastnäsite (bs) and calcite (cc).

compositional data for Kamthai britholite given in Wall *et al.* (1993) appear to be in error as the structural formula (Table 4; comp. 7) indicates significant *A*-site deficiencies and *B*-site excess with *A/B* ratios of 1.3. Patel *et al.* (2023a) have recognised 'magmatic' britholite and 'altered or secondary' britholite at Kamthai with the latter being similar in composition (Table 4; comp. 9) and texture to the britholite analysed in this work. The trend of compositions from 'magmatic' to 'secondary' hydroxylbritholite given by Patel *et al.* (2023a) is similar with decreasing Si, REE and F coupled with increasing Ca, P and OH. All britholite analysed in this study have low La/Ce ratios (0.48–0.56), whereas Patel *et al.* (2023a) have reported 'magmatic' La-enriched types with La/Ce ratios of 0.64–0.69 and 'altered types' with La/Ce ratios of 0.62–0.95.

Discussion

The objective of this contribution is not to provide a comprehensive genetic model for the Kamthai REE deposit, rather, the principal intent is to outline some mineralogical and broad textural features which are of genetic significance which have not been considered in previous investigations. Foremost of these is recognition of two textural varieties of daqingshanite i.e. granular and micro-ovoid, and evidence that the deposit is a carbothermal microbreccia formed in a least three genetic stages.

Origins of the daqingshanite parageneses

With respect to the granular type 1 variety of daqingshanite, BSE petrography demonstrates it has crystallised subsequent to altered britholite and monazite-(La) and prior to abundant carbocernaite (Figs 1–3). The anhedral-to-ovoid habit and heterogeneous compositions of both daqingshanite (Figs 3 and 4) and britholite (Fig. 8) suggest resorption and alteration during transport in the fluids which crystallised the host granular carbocernaite, baryte and bastnäsite. These assemblages are set in a matrix of Sr-bearing calcite (Fig. 1) and are considered to represent transported and disaggregated clasts within the carbothermal fluids which formed the Sr-bearing calcite. The latter is here not considered to be 'magmatic calcite' unlike the suggestion of Patel *et al.* (2023a, 2023b) on the basis of the high SrO content of the calcite (see below).

The microgranular ovoid-to-globular type 2 daqingshanite is found in discrete sub-angular clasts which in some instances also contain lamellae of carbocernaite (Fig. 7). These clasts are set in a relatively Sr-poor calcite (8–10 wt.% SrO) matrix compared to the calcite (11–13 wt.% SrO) which forms the host to the daqingshanite globules. The origins of the daqingshanite globules are clearly distinct from those of the granular variety and their sub-parallel orientation might initially suggest an exsolution

Table 4. Representative compositions of britholite.*

Wt.%	1	2	3	4	5	6	7	8	9
SiO$_2$	17.99	18.67	18.96	16.78	17.36	16.86	24.20	20.21	18.39
P$_2$O5	3.26	2.35	2.15	5.61	4.27	5.19	0.89	1.59	5.08
CaO	11.24	10.29	10.20	12.61	12.06	12.28	8.65	10.02	14.02
SrO	2.65	1.80	1.84	3.02	2.92	2.17	1.79	2.18	0.63
La$_2$O$_3$	15.01	16.91	17.17	16.47	14.69	16.58	18.87	21.47	23.71
Ce$_2$O$_3$	31.26	32.88	31.84	29.86	31.00	29.31	29.00	31.83	25.06
Pr$_2$O$_3$	3.22	3.06	3.25	2.92	3.16	3.42	2.60	2.64	1.29
Nd$_2$O$_3$	7.11	6.06	6.46	5.92	6.50	5.68	8.42	7.11	3.39
Sm$_2$O$_3$	0.85	0.98	1.09	0.95	0.72	0.89	0.72	-	-
F	0.89	0.90	0.39	1.04	0.75	0.85	1.52	2.00	0.15
Total	93.48	93.90	93.35	95.18	93.43	93.23	96.67	99.15	91.72
Structural formulae in apfu calculated on the basis of 8 cations									
Si	2.602	2.735	2.776	2.343	2.477	2.404	3.393	2.851	2.551
P	0.399	0.291	0.267	0.663	0.516	0.627	0.107	0.202	0.597
B site	3.001	3.026	3.043	3.006	2.992	3.031	3.500	3.053	3.147
Ca	1.742	1.615	1.600	0.848	1.843	1.876	1.300	1.514	2.083
Sr	0.222	0.153	0.156	0.440	0.420	0.179	0.146	0.178	0.051
La	0.801	0.914	0.927	0.848	0.773	0.872	0.976	1.117	1.213
Ce	1.655	1.763	1.707	1.526	1.619	1.530	1.489	1.644	1.273
Pr	0.170	0.163	0.173	0.149	0.164	0.178	0.133	0.136	0.065
Nd	0.367	0.317	0.338	0.295	0.331	0.289	0.422	0.358	0.168
Sm	0.042	0.049	0.055	0.046	0.035	0.044	0.035	-	-
A site	4.999	4.974	4.957	4.994	5.008	4.969	4.500	4.947	4.853
F	0.407	0.417	0.181	0.459	0.338	0.383	0.624	0.892	0.066
F/OH	0.686	0.715	0.221	0.848	0.511	0.620	1.659	8.259	0.007

*Compositions 1–3 are areas of high BSE in contrast relative to areas 4–6, respectively (this work); 7 Wall *et al.* (1993) average of 9 analyses; 8 'magmatic' britholite; and 9 altered britholite (Patel *et al.*, 2023a). '–' not detected.

origin from their host Sr-calcite. Unfortunately, there are no experimental phase equilibria which are relevant to these compositions. The texture exhibited is similar to that of 'chalcopyrite disease', which consists of micro-globules of chalcopyrite in a sphalerite host (Fig. 10). The origins of the texture have been debated widely and ascribed to exsolution, replacement or co-precipitation (Barton and Bethke, 1987; Nagase and Kojima, 1997; Tun and Aye, 2020). These investigations have typically ruled-out exsolution except for high-temperature metamorphosed ores and focused on hydrothermal processes. Exsolution is considered unlikely for the daqingshanite in calcite as the globules, although forming linear arrays, these arrays do not follow the rhombohedral calcite cleavage planes (see below). Nagase and Kojima (1997) have suggested that ellipsoidal chalcopyrite in sphalerite reflects extensive replacement whereas a triangular morphology indicates coprecipitation. On this basis, the daqingshanite globules could be interpreted as replacement features. Clearly, the daqingshanite globules at Kamthai have formed in a low temperature carbothermal environment which should facilitate replacement. Given that daqingshanite is an early crystallising phase it is also possible that cotectic crystallisation with Sr-calcite occurred, followed by subsolidus re-equilibration with recrystallisation along specific crystallographic planes in the calcite. Until further HRTEM investigations are undertaken the origins of the globular daqingshanite texture will remain enigmatic.

Some clasts containing microgranular daqingshanite globules are also characterised by trellis-like lamellae of carbocernaite (Fig. 7). These lamellae follow the rhombohedral cleavage of the calcite host and thus have morphological similarities with the trellis exsolution of ilmenite in magnetite (Haggerty 1996). Both Wall et al. (1993) and Patel et al. (2023a, 2023b) attribute the Kamthai trellis texture to exsolution of carbocernaite from a pre-existing Ca–Sr–Na–REE-carbonate solid solution. However, BSE imagery shows that the carbocernaite actually appears to have invaded the existing daqingshanite–calcite assemblage as carbocernaite lamellae can be seen clearly to cross-cut daqingshanite globules (Fig. 7b). The lamellae in some instances are not continuous and can also develop flame-like protrusions into the host calcite (Fig. 8), with symplectite-like intergrowths being developed in
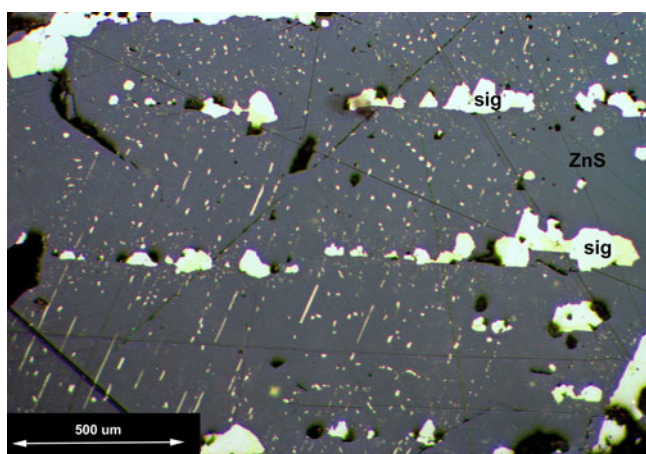
some cases. Regarding exsolution, it would seem highly improbable that exsolution of daqingshanite followed by a second exsolution of carbocernaite would occur. Further evidence for a replacement origin is that some carbocernaite lamellae contain small anhedral crystals of britholite, daqingshanite, baryte, and Mn–Al-bearing magnetite. These early-forming minerals (or antecrysts) appear to have been transported along the lamellae during their emplacement (Fig. 8). It is apparent that trellis carbocernaite is present only in some of the globular daqingshanite-bearing clasts and that both textural types of clast can occur juxtaposed. This observation implies that all of the globular daqingshanite-bearing clasts were formed at the same time, but only some were transported to an environment where carbocernaite-forming fluids were available to enter the calcite cleavage planes. Note that subsequently both types of clast were subjected to secondary replacement processes as illustrated in Fig 8b and that these were more intense in the clasts characterised by trellis lamellae. All clasts were subsequently mixed and cemented by Sr-calcite. In summary, it is proposed that the trellis-like carbocernaite-bearing clasts were not formed by exsolution and a replacement origin during transport is proposed.

Carbothermalite microbreccia formation

Standard optical and BSE petrographic observations (this work; Patel et al., 2023a, 2023b) show clearly that the Kamthai REE deposit as a whole does not exhibit the typical textures or mineralogy of primary magmatic carbonatites as defined by Mitchell and Gittins (2022). Such carbonatites are present only as clasts (see below) within the deposit, which is actually a breccia consisting of veins and clasts with a wide range of textural and mineralogical characteristics. Many of the earlier-formed clasts have been subjected to low-temperature secondary replacement processes (Uphadyay et al., 2021).

The Sarnu-Dandhali complex is similar to other subvolanic nephelinite-phonolite complexes, such as Freemans Cove (Mitchell and Platt, 1984), Balcones (Barker et al., 1987) and Hegau-Urach (Engelhardt and Weiskirchner, 1963), although REE deposits have not been found associated with these complexes. Unfortunately, plutonic members of the Sarnu-Dandhali complex are not well-exposed. The observations of Bhushan and Kumar (2013) have shown that the 'carbonatite plug' and the REE-enriched veins at Kamthai are associated geographically with cross-cutting younger phonolite dykes but there are no evident genetic relationships with these subvolcanic silicate rocks. As a direct mantle origin for these carbothermalites is extremely unlikely, it is highly probable that the REE-rich veins are derived from unexposed late stage differentiates of plutonic members (ijolite suite rocks) of the complex. Evidence in support of this hypothesis is the occurrence of one Ba-rich carbonate dyke intruding an ijolite breccia. Further geological and geophysical exploration of the area is obviously required.

From these observations it is proposed that the deposit formed in at least three stages: (1) formation of magmatic calcite carbonatite by fractional crystallisation of an as yet undetermined parental magma in a plutonic environment; (2) differentiation of the calcite carbonatite-forming magma to low temperature carbothermalite-forming vein deposits coupled with autobrecciation; (3) formation of late-stage veins and replacement of pre-existing clasts by 'secondary' LREE-enriched carbothermal fluids mixed with exogenous water. The paragenetic sequence and major mineral assemblages associated with the three stages are summarised in Fig. 11.
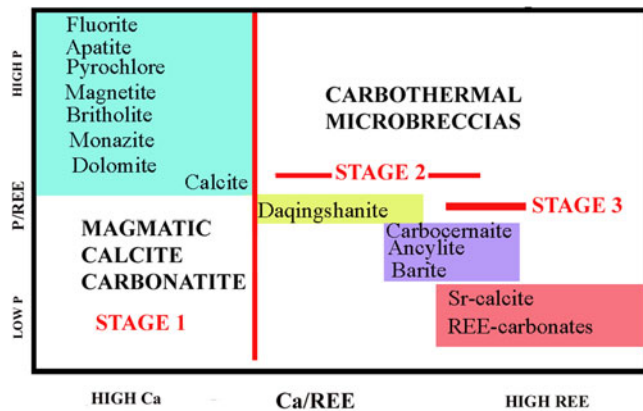

Figure 10. Reflected light image of 'chalcopyrite disease' which consists of micro-globular chalcopyrite (pale yellow) set in a matrix of sphalerite (ZnS). The coarse grained material is siegenite (sig). Compare the texture with that of daqingshanite illustrated in Fig. 6 of this work. This example of 'chalcopyrite disease' is from the Erglodd Mine, Mid Wales (image courtesy of Dr. John Mason and the Museum of Wales).

Figure 11. Paragenetic sequence of mineral assemblages in the stages of the evolution of the Kamthai carbothermalite.

The genetic model is similar to the common magmatic to hydrothermal transition proposed to explain the genesis of ore deposits associated with plutonic granitoids such as porphyry copper deposits (Audétat and Edmonds, 2020) or critical metal-bearing peralkaline granites (Ronchi *et al.*, 2011) This model considers that crystallising plutons reach fluid saturation during crystallisation of the parental magma with subsequent continuous separation of low-temperature hydrothermal fluids which are commonly accompanied by brecciation. A similar model for 'late-forming' REE deposits associated with alkaline rock carbonatite complexes has been suggested by Wall and Mariano (1996) and Wall and Zaitsev (2004). The magmatic-to-carbothermal transition proposed by Mitchell and Gittins (2022) is an analogous process involving carbonate-rich fluids rather than hydrothermal fluids.

Stage 1 is represented by clasts of coarse-grained magmatic calcite carbonatite which contains accessory fluorite, magnetite and minor dolomite (Fig. 12). Calcite in these clasts ranges in texture from allotriomorphic granular to prismatic laths. These calcite are enriched in MnO (4–5 wt.%) and poor in SrO (1–2 wt.%) relatively to carbothermal calcite. The presence of interstitial late-

stage miarolitic cavities, which are not secondary replacement features, containing intergrowths of carbocernaite, baryte and ancylite demonstrates that carbothermalite-forming fluids were present in the later stages of crystallisation of the calcite carbonatite-forming magma (Fig. 12), and that REE enrichment is a primary fractional crystallisation process. Other clasts representing stage 1 material are pyrochlore-apatitites (Fig. 13) similar to those found in magmatic carbonatites at Good Hope, St. Honoré and Panda Hill (Mitchell *et al.*, 2020). This observation suggests that apatite forms only in stage 1 and primary britholite probably also crystallised at this time (700–900°C; Mollé *et al.*, 2021). Thus, the sequence of P-bearing minerals at Kamthai is apatite → britholite → daqingshanite. Clasts containing abundant magnetite as suggested by Uphadyay *et al.* (2021) do not appear to be common.

Stage 2 represents brecciation of stage 1 calcite carbonatites by several generations of granular type 1 daqingshanite–carbocernaite carbothermalite-forming fluids formed during the initial stages of the magmatic to carbothermal transition. Type 2 daqingshanite-bearing rocks formed at this time and these were also fragmented by the continuing evolving fluids, resulting in auto-brecciation and cementation of all of these diverse clasts in residual Sr-calcite-forming fluids (Fig. 7). Stage 3 represents residual carbothermal fluids undergoing further evolution and becoming enriched in La relative to Ce and other REE together with the mixing of exogenous water enriched in O^{18} as shown by Uphadyay *et al.* (2021). These fluids, which can be considered as carbohydrothermal fluids (Mitchell, 2005) invaded, and altered pre-existing breccias, created new breccias and deposited a wide variety of Mn and Fe bearing carbonates together with La-enriched REE fluorocarbonates such as bastnäsite-(La) (Fig. 14).

An important conclusion of the above model is that the bulk compositions of none of the rocks forming the Kamthai REE deposit represent liquid compositions and that the heterogeneous mineral assemblages present cannot represent equilibrium assemblages. Hence attempts to reconstruct the 'hydrothermal fluid composition' as attempted by Patel *et al.* (2023a) are not realistic. In addition, the partition coefficients of Chebotarev *et al.* (2022)
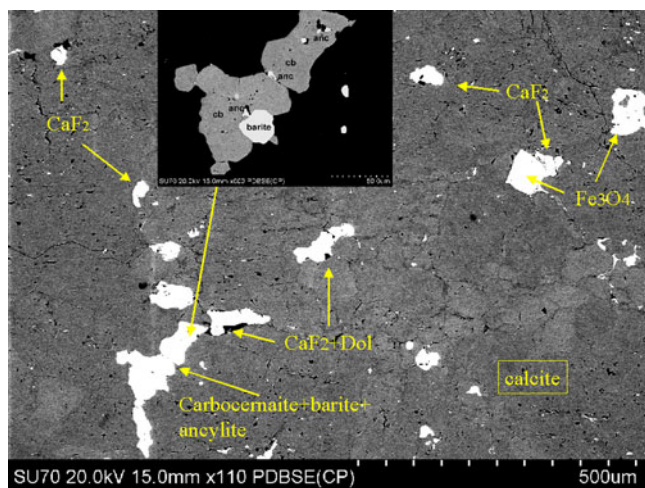

Figure 12. BSE image of primary calcite carbonatite with late stage fluorite, carbocernaite, baryte and ancylite (see the inset). Primary magnetite is also present. Note that the primary calcite exhibits variable but minor compositional variation as shown by the differing BSE contrast. Dolomite is present in trace amounts.
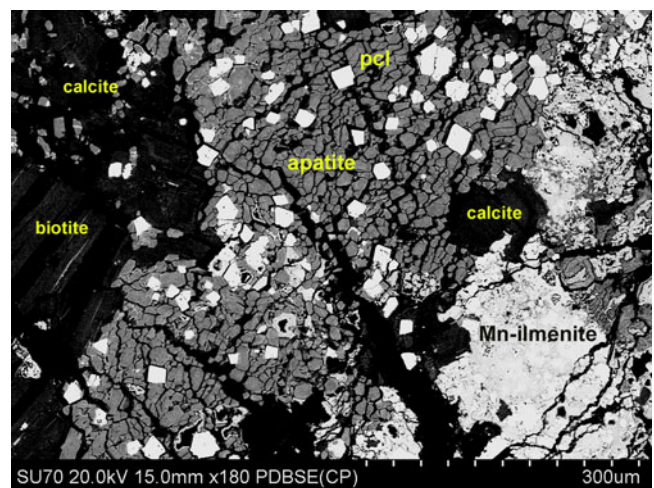

Figure 13. BSE image of pyrochlore (pcl) apatitite clast undergoing disaggregation during formation of stage 3 carbothermalite microbreccia. The clast, now set in secondary carbo(hydro)thermal calcite, is derived from stage 1 primary calcite carbonatite. Also present are secondary biotite and Mn-ilmenite.
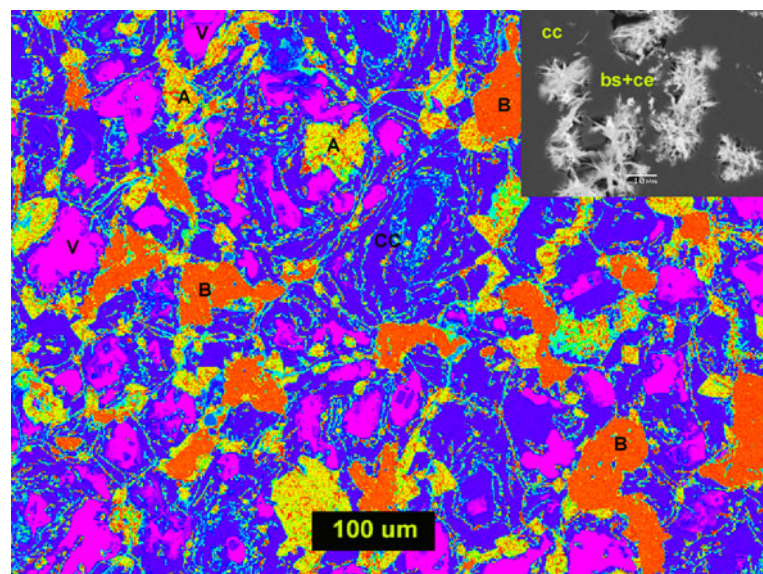
Figure 14. False colour BSE image of the texture of typical stage 3 carbothermalite microbreccia with clasts of stage 2 baryte (B) and ancylite (ANC) set in porous (V) very complex stage 3 matrix of diverse Mn–Sr carbonates and iron oxide/hydroxides with fine grained REE-minerals including bastnäsite-(La), synchysite-(La) (bs) and cerite (ce) (see inset).

used by Patel *et al.* (2023a) were derived from melt compositions that were highly enriched in Na_2O (mainly 20–26 wt.%) and formed at temperatures of 650–900°C, i.e. well above those expected for the magmatic to carbothermal transition (<400°C) and stability of Na–REE–Sr carbonates (i.e. 100–500°C, Perry and Gysi, 2018; Louvel *et al.*, 2022).

Conclusions

The Kamthai REE deposit is best described as a low-temperature carbothermalite microbreccia consisting of a wide variety of clasts resulting from the autobrecciation of rocks formed during, and after, the magmatic to carbothermal transition of an undetermined parental carbonatite-forming magma. Many clasts have been replaced by late-stage La-enriched carbothermal fluids mixed with exogenous water during the final low-temperature stage of evolution of the deposit.

Daqingshanite at Kamthai occurs as two paragenetic types: primary granular coarse grained and coexisting with primary carbocernaite and baryte and bastnäsite; and micro-ovoid globules of as yet undetermined origin.

Carbocernaite forming trellis-type lamellae in Sr-calcite clasts does not represent exsolution and is considered as a replacement texture.

References

Amores-Casals S., Gonçalves A.O., Melgarejo J.C. and Molist J.M. (2020) Nb and REE distribution in the Monte Verde carbonatite-alkaline-agpaitic complex (Angola). *Minerals*, **2020**, 10, doi:10.3390/min100100005.

Appleton J.D., Bland D.J., Nancarrow P.H., Styles M.T., Mambwe S.H. and Zambezi P. (1992) The occurrence of daqingshanite-(Ce) in the Nkombwa Hill carbonatite, Zambia. *Mineralogical Magazine*, **56**, 419–422.

Audétat A. and Edmonds M. (2020) Magmatic-hydrothermal fluids. *Elements*, **16**, 401–406.

Barker D.S., Mitchell R.H. and McKay D. (1987) Late Cretaceous nephelinite to phonolite magmatism in the Balcones province, Texas. *Geological Society of America Special Paper*, **215**, 293–304.

Barton P.B. and Bethke P.M. (1987) Chalcopyrite disease in sphalerite: Pathology and epidemiology. *American Mineralogist*, **72**, 451–467.

Bhushan S.K. and Kumar A. (2013) First carbonatite hosted REE deposit from India. *Journal of the Geological Society of India*, **81**, 41–60.

Bushan S.K. (2015) Geology of the Kamthai rare earth deposit. *Journal of the Geological Society of India*, **85**, 537–546.

Chakhmouradian A.R., Cooper M.A., Reguir E.P. and Moore M.A. (2017) Carbocernaite from Bear Lodge, Wyoming: Crystal chemistry. paragenesis and rare-earth fractionation on a microscale. *American Mineralogist*, **102**, 1340–1352.

Chebotarev D.A., Wohlgemuth-Überwasser C. and Tong H. (2022) Partitioning of REE between calcite and carbonatitic melt containing P, S, Si at 650–900°C and 100MPa. *Scientific Reports*, **12**, 3320.

Dowman E., Wall F. and Treloar P. (2022) A comparison of the fenites at the Chilwa Island and Kangankunde carbonatite complexes, Malawi. *Mineralogical Magazine*, **87**, 300–322.

Engelhardt W. and Weiskirchner W. (1963) Einfürung zu den Exkursionen der Deutschen Mineralogischen Gesellschaft zu den Vulkanschlotan der Schwäbischen Alb und vin den Hegau. *Forschritte der Minerologie*, **40**, 5–28.

Haggerty S.E. (1996) Oxide textures: a mini-atlas. Pp. 125–219 in: *Oxide Minerals: Petrologic and Magnetic Significance* (Donald H. Lindsley, editor). Reviews in Mineralogy and Geochemistry, 25. Mineralogical Society of America, Washington DC.

Hughes J.M and Yunxiang N. (1994) A high-precision crystal structure refinement of daqingshanite-(Ce) from the Nkombwa Hill carbonatite, Zambia. *Mineralogical Magazine*, **58**, 493–496.

Louvel M., Etschmann, B., Qiushi G., Testemale D. and Brugger J. (2022) Carbonate complexation enhances transport of rare earth elements in alkaline fluids. *Nature Communications*, **13**, 1456 doi.org/10.1038/s41467-022-28943-z.

Mahala M.K. and Ray J.S. 2022. Age and geochemistry of the Kamthai carbonatites, Rajasthan, western India. *EGU General Assembly* 2022 *Vienna Austria*, EGU22, 10951, doi.org/10.5194/egusphere-egu22-105551,2022.

Mitchell R.H. (1995) *Kimberlites, Orangeites and Related Rocks*. Plenum Press, New York.

Mitchell R.H. (2005) Carbonatites and carbonatites and carbonatites. *The Canadian Mineralogist*, **43**, 2049–2068.

Mitchell R.H. and Gittins J. (2022) Carbonatites and carbothermalite: A revised classification. *Lithos*, **430**, 106861, doi:10.1016/j.lithos.2022.106861.

Mitchell R.H. and Platt R.G. (1984) The Freemans Cove volcanic suite: field relations petrochemistry and tectonic setting of nephelinite-basanite volcanism associated with rifting in the Canadian Arctic archipelago. *Canadian Journal of Earth Sciences*, **21**, 428–436.

Mitchell R.H., Wahl R. and Cohen H. (2020) Mineralogy and genesis of pyrochlore apatitite from the Good Hope carbonatite, Ontario: A potential niobium deposit. *Mineralogical Magazine*, **84**, 81–91.

Mollé V., Gaillard F., Nabyl Z., Tuduri J. and Di Carlo I. (2021) Crystallization sequence of a REE-rich carbonatite melt: an experimental approach. *Comptes Rendus Géoscience – Series de la Planète*, **353**, 217–231.

Nagase T. and Kojima S. (1997) A SEM examination of the chalcopyrite disease texture ad its genetic implications. *Mineralogical Magazine*, **61**, 80–97.

Patel A.K., Upadhyay D., Mishra B. and Pruseth K.L. (2023a) Reconstruction of hydrothermal fluid composition of the Kamthai carbonatite complex, India using a lattice strain model: Implications for LREE/HREE fractionation. *Lithos*, **444–445**, 107097.

Patel A.K., Upadhyay D., Mishra B. and Pruseth K.L. (2023b) Magmatic rare earth mineralization and secondary fluid-assisted redistribution in the Kamthai carbonatite complex, NW India. *Lithos*, **456–457**, 107294.

Perry E.P. and Gysi A.P. (2018) Rare earth elements in mineral deposits: speciation in hydrothermal fluids and partitioning in calcite. *Geofluids*, **2018**, doi.org/10.1155/2018/5382480.

Risedorf S. (2023) *Investigations of the Sheep Creek carbonatite, Ravelli County, Montana.* Montana Technical University Butte, Montana, USA. Unpublished M.Sc. Thesis, 151 pp.

Ronchi L.H., Bastos Neto A.C., Gedoz S.C., Weber M.L., Pereira V.P. and Andrek M. (2011) A transição magmático-hidrotermal registrada por inclusões fluidas no albito-granito de núcleo, Mina Pitinga, Amazonas. Pp. 71–88 in: *Contribuições à Metalogenia do Brasil* (J.C. Frantz, J.M. Charão and H. Jost, editors). CPRM – IGEO – UFRGS.

Shi N., Ma Z. and Peng Z. (1982) The crystal structure of carbocernaite. *Kexue Tongbao*, **27**, 76–80 [in Chinese].

Sitnikova M.A., Do Cabo V., Wall, F. and Goldmann S. (2021) Burbankite and pseudomorphs from the Main intrusion calcite carbonatite, Lofdal, Namibia: Association, mineral composition and Raman spectroscopy. *Mineralogical Magazine*, **85**, 496–513.

Tun M.M. and Aye M.T. (2020) Origin of chalcopyrite disease from lead-zinc-silver-gold mineralization of the Scharchet area, Thabeikkyin Township, Mandalay Region, Myanmar. *International Journal of Scientific Research in Multi disciplinary Studies*, **6**, 81–86.

Uphadyay D., Monndal S., Patel A.K., Mishra B., Pruseth K.L. and Bhushan S.K. (2021) Rare earth element precipitation induced by non-redox transformation of magnetite to hematite: Microtextural and geochemical evidence from the Kamthai carbonatite complex, western India. *Lithos*, **400–401**, 106381.

Wall F. and Mariano A.N. (1996) Rare earth minerals in carbonatites: a discussion centred on the Kangankunde Carbonatite, Malawi. Pp. 193–225 in: *Rare Earth Minerals: Chemistry, Origin and Ore Deposits.* The Mineralogical Society Series, 7 (A.P. Jones, F. Wall, and T.C. Williams, editors). Chapman & Hall, London.

Wall F. and Zaitsev A.N. (2004) Rare earth minerals in Kola carbonatites. Pp. 341–373 in: *Phoscorites and Carbonatites from Mantle to Mine: the Key Example of the Kola Alkaline Province* (F. Wall and A.N. Zaitsev, editors). Mineralogical Series 10, Mineralogical Society, London, UK.

Wall F., Le Bas M.J. and Srivastava R.K. (1993) Calcite and carbocernaite exsolution and eutectic textures in a Sr, REE-rich carbonatite dyke from Rajasthan, India. *Mineralogical Magazine*, **57**, 495–513.

Ximen L. and Peng Z. (1985) Crystal structure of daqingshanite. *Geochemistry (China)*, **4**, 89–96.

Yingchen R., Lulu X. and Zhizhong P. (1983) Daqingshanite - a new mineral recently discovered in China. *Geochemistry (China)*, **2**, 180–184.

Zaitsev A.N., Wall F. and Le Bas M.J. (1998) REE-Sr-Ba minerals from the Khibina carbonatites, Kola Peninsula, Russia: their mineralogy, paragenesis and evolution. *Mineralogical Magazine*, **62**, 225–250.